The LHC as a Neutrino-Ion Collider

Max Fieg[1], Tommaso Giani[2,3], Peter Krack[2,3] Giacomo Magni[2,3],
Toni Makela[4], Tanjona Rabemananjara[2,3], and Juan Rojo[2,3],

[1] *UC Irvine*
[2] *Department of Physics and Astronomy, Vrije Universiteit, NL-1081 HV Amsterdam*
[3] *Nikhef Theory Group, Science Park 105, 1098 XG Amsterdam, The Netherlands*
[4] *IPJ*

Abstract

Proton-proton collisions at the LHC produce a collimated beam large flux of high-energy neutrinos, which until recently escaped detection and hence we not used for physics. Detection and analysis of these far-forward LHC neutrinos is taking now place at the FASERν and SND@LHC experiments, and would be uniquely scrutinized at the proposed Forward Physics Facility (FPF). In this work we demonstrate that exploiting this high-energy far-forward neutrino beam provides new constraints on the quark and gluon substructure of nucleons and nuclei. We generate projections for inclusive and charm (dimuon) deep-inelastic scattering (DIS) structure functions at cross-sections for all ongoing and planned far-forward LHC neutrinos experiments, including the expected systematic uncertainties. By means of both the xFitter and NNPDF frameworks we quantify the impact of the FPF measurements on proton and nuclear structure, showing stringent constraints specially in quark flavour separation. Our analysis demonstrates that instrumenting the far-forward region to exploit the HL-LHC neutrino fluxes effectively realises a Neutrino-Ion Collider with center of mass energy around 100 GeV at CERN, fully complementary and operating concurrently to the Electron-Ion Collider in the US.

Contents

1 Recap of DIS kinematics

The double-differential cross-section for neutrino-nucleus scattering can be decomposed in terms of three independent structure functions $F_i^{\nu A}(x,Q^2)$ with $i=1,2,3$. Focusing on the charged-current (CC) scattering case, mediated by the exchange of a W^+ weak boson, the differential cross section reads

$$\frac{d^2\sigma^{\nu A}(x,Q^2,y)}{dxdy} = \frac{G_F^2 s/2\pi}{\left(1+Q^2/m_W^2\right)^2}\left[(1-y)F_2^{\nu A}(x,Q^2)+y^2xF_1^{\nu A}(x,Q^2)+y\left(1-\frac{y}{2}\right)xF_3^{\nu A}(x,Q^2)\right], \quad (1.1)$$

where $s=2m_N E_\nu$ is the neutrino-nucleon center of mass energy squared, m_N is the nucleon mass, E_ν is the incoming neutrino energy, and the inelasticity y is defined as $y=Q^2/(2xm_nE_\nu)$. For the time being we are neglecting target mass corrections. An analogous expression holds for antineutrino scattering, mediated by

the exchange of a W^- weak boson, with the only difference being a sign change in front of the parity-violating structure function xF_3,

$$\frac{d^2\sigma^{\bar{\nu}A}(x,Q^2,y)}{dxdy} = \frac{G_F^2 s/2\pi}{\left(1+Q^2/m_W^2\right)^2}\left[(1-y)F_2^{\bar{\nu}A}(x,Q^2) + y^2 xF_1^{\bar{\nu}A}(x,Q^2) - y\left(1-\frac{y}{2}\right)xF_3^{\bar{\nu}A}(x,Q^2)\right] . \quad (1.2)$$

While the differential cross-section depends on three kinematic variables, (x, Q^2, y), the structure functions themselves depend only on x and Q^2. Furthermore, both the cross-section and the structure functions depend on the atomic mass number A of the target nucleus via nuclear modifications of the free-nucleon structure functions.

Alternatively, Eq. (1.1) can be expressed in terms of the longitudinal structure function $F_L^{\nu A}(x,Q^2)$ defined by $F_L = F_2 - 2xF_1$, leading to

$$\frac{d^2\sigma^{\nu A}(x,Q^2,y)}{dxdy} = \frac{G_F^2 s/4\pi}{\left(1+Q^2/m_W^2\right)^2}\left[Y_+ F_2^{\nu A}(x,Q^2) - y^2 F_L^{\nu A}(x,Q^2) + Y_- xF_3^{\nu A}(x,Q^2)\right] , \quad (1.3)$$

where $Y_\pm = 1 \pm (1-y)^2$ and with a counterpart expression for anti-neutrino scattering,

$$\frac{d^2\sigma^{\bar{\nu}A}(x,Q^2,y)}{dxdy} = \frac{G_F^2 s/4\pi}{\left(1+Q^2/m_W^2\right)^2}\left[Y_+ F_2^{\bar{\nu}A}(x,Q^2) - y^2 F_L^{\bar{\nu}A}(x,Q^2) - Y_- xF_3^{\bar{\nu}A}(x,Q^2)\right] , \quad (1.4)$$

Expressing the differential cross-section as in Eq. (1.3) is advantageous because in the parton model (and in perturbative QCD at leading order) the longitudinal structure function vanishes, $F_L^{\nu A}(x,Q^2) = 0$. The combination of neutrino and antineutrino measurements makes possible disentangling the different structure functions, for example the cross-section difference

$$\frac{d^2\sigma^{\nu A}(x,Q^2,y)}{dxdy} - \frac{d^2\sigma^{\bar{\nu}A}(x,Q^2,y)}{dxdy} = \frac{G_F^2 s Y_-}{4\pi\left(1+Q^2/m_W^2\right)^2}\left[xF_3^{\nu A}(x,Q^2) + xF_3^{\bar{\nu}A}(x,Q^2)\right] , \quad (1.5)$$

is proportional to the parity-violating structure function xF_3 averaged over neutrinos and antineutrinos.

When both the momentum transfer squared Q^2 and the hadronic final-state invariant mass W given by

$$W^2 = m_N^2 + Q^2\frac{(1-x)}{x} , \quad (1.6)$$

are large enough, $Q^2 \gtrsim$ few GeV^2 and $W \gtrsim 2$ GeV respectively, we find ourselves in the deep-inelastic scattering region where structure functions can be evaluated in perturbative QCD in terms of a factorised convolution of process-dependent partonic scattering cross-sections and of process-independent parton distribution functions,

$$F_i^{\nu A}(x,Q^2) = \sum_{j=q,\bar{q},g}\int_x^1 \frac{dz}{z}\, C_{i,j}^{\nu N}(z,\alpha_s(Q^2)) f_j^{(A)}\left(\frac{x}{z},Q^2\right) , \quad i = 2,3,L , \quad (1.7)$$

where j is an index that runs over all possible partonic initial states and $C_{i,j}^{\nu N}$ is the process-dependent (but target-independent) coefficient function. The latter can be expressed as a series expansion in powers of the strong coupling $\alpha_s(Q^2)$,

$$C_{i,j}^{\nu N}(z,\alpha_s(Q^2)) = \sum_{k=0}^{m}\left(\alpha_s(Q^2)\right)^k C_{i,j}^{\nu N(k)}(z) . \quad (1.8)$$

The leading-order ($k = 0$) term is independent of α_s since the Born scattering is mediated by the weak interaction. At leading order and considering a proton target, $n_f = 4$ active quark flavours, neglecting charm mass effects and assuming a diagonal CKM matrix, we can express the $F_2^{\nu p}$ and $xF_3^{\nu p}$ structure functions as follows

$$\begin{aligned}
F_2^{\nu p}(x,Q^2) &= 2x\left(f_{\bar{u}} + f_d + f_s + f_{\bar{c}}\right)(x,Q^2) , \\
F_2^{\bar{\nu} p}(x,Q^2) &= 2x\left(f_u + f_{\bar{d}} + f_{\bar{s}} + f_c\right)(x,Q^2) , \\
xF_3^{\nu p}(x,Q^2) &= 2x\left(-f_{\bar{u}} + f_d + f_s - f_{\bar{c}}\right)(x,Q^2) , \\
xF_3^{\bar{\nu} p}(x,Q^2) &= 2x\left(f_u - f_{\bar{d}} - f_{\bar{s}} + f_c\right)(x,Q^2) .
\end{aligned} \quad (1.9)$$

The corresponding expressions for a neutron target and or isoscalar target can be obtained from isospin symmetry, for instance the LO structure functions for neutrino-neutron scattering are

$$\begin{aligned} F_2^{\nu n}(x,Q^2) &= 2x\left(f_{\bar{d}}+f_u+f_s+f_{\bar{c}}\right)(x,Q^2)\,, \\ F_2^{\bar{\nu} n}(x,Q^2) &= 2x\left(f_d+f_{\bar{u}}+f_{\bar{s}}+f_c\right)(x,Q^2)\,, \\ xF_3^{\nu n}(x,Q^2) &= 2x\left(-f_{\bar{d}}+f_u+f_s-f_{\bar{c}}\right)(x,Q^2)\,, \\ xF_3^{\bar{\nu} n}(x,Q^2) &= 2x\left(f_d-f_{\bar{u}}-f_{\bar{s}}+f_c\right)(x,Q^2)\,. \end{aligned} \tag{1.10}$$

2 DIS pseudo-data generation

The first goal is to produce projections for DIS pseudo-data at the FPF based on some idealised detector concepts and some initial choice of neutrino fluxes e.g. [1]. This requires a knowledge of the detector geometry and material, as well as of the double-differential neutrino interaction cross-section. Since we aim to produce pseudo-data binned in (x, Q^2), for each simulated event we need to determine the final-state kinematics.

Specifically, we would like to evaluate the number of charged-current neutrino interaction events within the detector volume in different bins of the incoming neutrino energy E_ν, the Bjorken variable x and the momentum transfer square Q^2,

$$N_{\rm ev}(E_\nu, x, Q^2)\,, \tag{2.1}$$

for some binning in these three kinematic variables. This can be evaluated as

$$N_{\rm ev}(E_\nu, x, Q^2) = \frac{d^2\sigma^{\nu A}(x,Q^2,y)}{dxdy}\mathcal{L}(E_\nu)\,, \tag{2.2}$$

where $\mathcal{L}(E_\nu)$ is the incoming neutrino luminosity which accounts for the detector geometry and material density. Eq. (2.2) can be integrated to determine the actual number of events within the bin boundaries.

We start with a perfect detector.

For bins in x, Q^2, E_ν, we start with the differential cross section, $\frac{d^2\sigma(x,Q^2,E_\nu}{dxdQ^2})$ [pb GeV^{-2}] as output from `YADISM` and convolve with the neutrino flux, $\frac{dN_\nu}{dE_\nu}$. So for a detector with n_T nuclear target density and L_T length, we calculate the event rate per bin as

$$N_{\rm ev}/{\rm bin} = n_T L_T \int_{Q^2_{min}}^{Q^2_{max}} \int_{x_{min}}^{x_{max}} \int_{E_{\nu,min}}^{E_{\nu,max}} \frac{dN_\nu}{dE_\nu}\left(\frac{d^2\sigma(x,Q^2,E_\nu)}{dxdQ^2}\right) dQ^2 dx dE_\nu. \tag{2.3}$$

Using a MC integration, we can calculate $N_{\rm ev}/{\rm bin}$ by sampling N points in x, Q^2, E_ν space such that $0 < y = \frac{Q^2}{2m_N E_\nu x} < 1$ and integrating over the bin.

$$N_{\rm ev}/{\rm bin} \approx n_T L_T \frac{(Q^2_{max}-Q^2_{min})(x_{max}-x_{min})(E_{\nu,max}-E_{\nu,min})}{N} \times \sum_i^N f(x_i, Q_i^2, E_{\nu,i}) \tag{2.4}$$

where $f(x_i, Q_i^2, E_{\nu,i}) = \frac{dN_\nu}{dE_{\nu,i}}\left(\frac{d^2\sigma(x_i,Q_i^2,E_{\nu,i})}{dxdQ^2}\right)$.

The statistical uncertainty for each bin is then defined by a Gaussian distribution with fractional uncertainty $1/\sqrt{N{\rm ev/bin}}$, i.e. $\delta N_{\rm ev}/{\rm bin} = \sqrt{N_{\rm ev}}/{\rm bin}$

Following this prescription, we can produce plots which characterize the event rate for a particular neutrino species at a particular experiment.

Results for FASERν2 can be found here. The .txt files will display which neutrino species was considered, and also compile experimental geometries and target details in the header. In the sub-folder summaries, plots can be found which show the event rate in x, Q^2 space, integrating over the entire neutrino spectrum. The event rate for muon neutrinos at FASERν2 is shown in Fig 2.1.

2.1 Systematic Effects on Pseudodata

We now wish to understand the impact of systematic uncertainties on the event rate in (x, Q^2, E_ν) space. For each experiment, the observables E_l, E_h, θ are related to (x, Q^2, E_ν) by

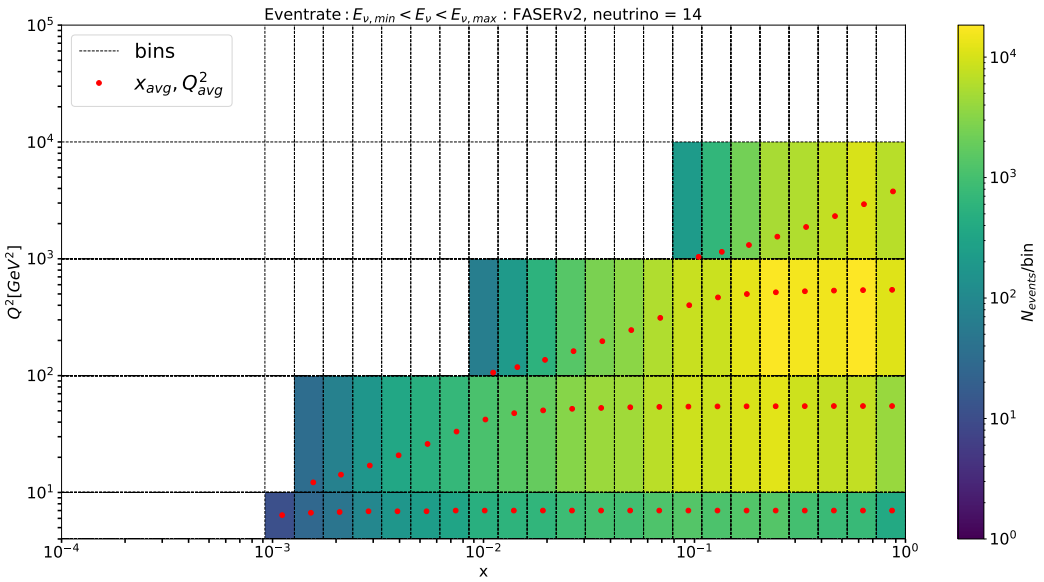

Figure 2.1. Event rate per bin for muon neutrinos at FASERν2. Bins are denoted by dashed grid, and the red dot indicates the weighted average of x, Q^2 points in each bin. The total number of muon neutrino events calculated is $\approx 2.6 \times 10^5$. Note that bins were chosen somewhat arbitrarily, and can be iterated to improve PDF fits

$$\begin{aligned} E_\nu &= E_l + E_h \\ Q^2 &= 4E_l E_\nu \sin^2\theta/2 \\ x &= \frac{Q^2}{2m_N(E_\nu - E_l)}. \end{aligned} \tag{2.5}$$

We wish to sample over the space of observables, (E_l, E_h, θ), perform cuts based on detector performance, calculate the event rates, and then smear this sampling according to experimental uncertainties to estimate the uncertainty on the event rate.

Taking FASERν2 as an example, we can write the experimental cuts and uncertainties as

$$\begin{aligned} 100 < E_l < E_{\nu,\max}, \delta E_l = 30\% \\ 100 < E_h < E_{\nu,\max}, \delta E_h = 50\% \\ 0 < \theta < \tan^{-1}(0.5), \delta\theta = 1 \text{ mrad} \end{aligned} \tag{2.6}$$

We first generate a MC dataset, D_0, over this space with $N = 10^7$ samples and calculate x, Q^2, E_ν for each event, removing samples with $y > 1$. We then integrate according to Eq. 2.4 to produce a distribution of events with bins in x, Q^2, E_ν. We then smear each sample according to a Gaussian distribution with widths given by Eq. 2.6 to produce a new data set D_i and repeat to produce $M = 10$ event distributions($M > 10$ can later be used, but $M = 10$ appears to be stable). For each bin we take the standard deviation to produce the systematic errors per bin (denoted as "N_sys_errs" in files named "binned_sys-events... .txt" here).

For FASERν2, the systematic errors typically dominate over statistical errors, at about 10%.

3 Experimental acceptance performance

AdvSND

- The detectors will be able to track muons that have energy greater than 20 GeV (the values for the other charged leptons remain to be determined) with an acceptance angle of 100 mrad for the muons and 500 mrad for the both electrons and tau.

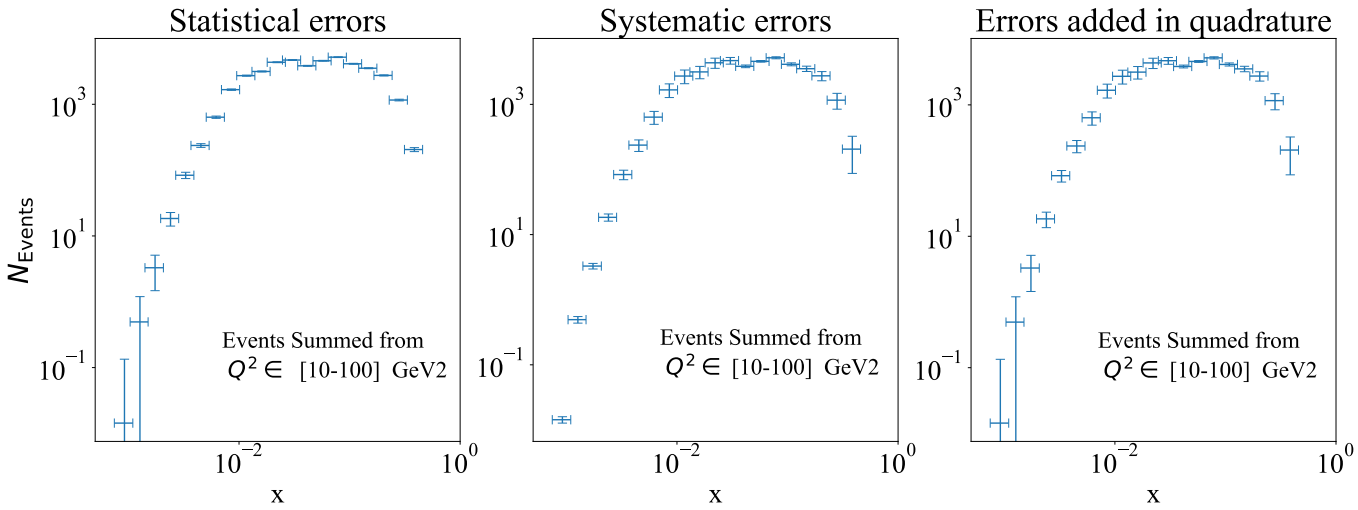

Figure 2.2. Event rates with error bars at FASERν2 for $\nu_\mu N \to \mu^- X$ summed over Q^2. The error bars along the x-axis showing the width of the x-bins, and are not showing any type of error.

- In addition, the information on the charge of the outgoing leptons can also be accessed.
- It should also be possible to reconstruct the hadronic final states by measuring the total energy.

FLArE

- The detectors will be able to detect electrons with energy up to 1 TeV and an acceptance angel as high as 0.5 rad. For the muons, the detectors will only be able to track them up to 1.5 GeV with a scattering angle reaching up to 0.4 mrad. The reconstruction of the tau's angle and energy instead will be very difficult. However, it might be possible to find the vertex of a particular tau decay if fine position resolution is achieved.
- With the current baseline design of the detector, it will not be possible to access the information on the sign of the charged leptons.
- It should also be possible to reconstruct the hadronic final states but the reconstruction efficiency and particles will depend on the type of particles. It is expected that the final states hadrons will be dominated by pions, protons, and neutrons.
- Regarding the systematic errors on the charged lepton energy and scattering angle, it is expected to get 5% energy resolution for electrons and about 15 mrad in angular resolution. Due to the large missing energy in the detector, 30% energy resolution is probably achievable for muons with about 5 mrad angular resolution.

4 Impact in proton PDF fits

Once we have generated pseudo-data for the neutrino DIS charged-current structure functions in bins of (x, Q^2, y), and assuming that uncertainties are purely of statistical origin, we can assess their impact on proton PDFs. At a first step we neglect nuclear effects and treat data as corresponding to a free isoscalar nucleon with $A = 1$.

The expected impact of the FPF data on global PDF fits is assessed by a profiling procedure [2–5], based on minimizing the function

$$\chi^2 = \sum_{i=1}^{N_{\text{bins}}} \frac{\left(\sigma_i^{\text{pd}} + \Gamma_i^{\alpha,\text{pd}} b_\alpha^{\text{pd}} - \sigma_i^{\text{th}} - \Gamma_i^{\beta,\text{th}} b_\beta^{\text{th}}\right)^2}{\Delta_i^2} + \sum_\alpha (b_\alpha^{\text{pd}})^2 + \sum_\beta (b_\beta^{\text{th}})^2 \,. \tag{4.1}$$

Here the pseudodata σ_i^{pd} is obtained from the central theoretical prediction σ_i^{th} for each bin i out of N_{bins} by varying it with the statistical uncertainties δ_i^{stat}, obtained in the procedure described in Section 2, as

$\sigma_i^{\rm pd} = \sigma_i^{\rm th}(1 + r_i \delta_i^{\rm stat})$, with r_i a univariate Gaussian random number. The correlated uncertainties for the pseudodata and the theoretical prediction are contained in the nuisance parameter vectors $b^{\rm pd}$ and $b^{\rm th}$, respectively, and the uncorrelated uncertainties in Δ_i. Their effect on $\sigma^{\rm th}$ and $\sigma^{\rm pd}$ is described by the matrices $\Gamma_i^{\rm pd}$ and $\Gamma_i^{\rm th}$. The indices α and β then run over the uncertainty nuisance parameters for the pseudodata and the theoretical prediction, respectively. The nuisance parameter values $b^{\rm th(min)}$ that minimize Eq. (4.1) give the central PDFs f_0' optimized to the profiled dataset in the form

$$f_0' = f_0 + \sum_\beta b_\beta^{\rm th(min)} \left(\frac{f_\beta^+ - f_\beta^-}{2} - b_\beta^{\rm th(min)} \frac{f_\beta^+ + f_\beta^- - 2f_0}{2} \right), \tag{4.2}$$

where f_0 is the original central PDF and the up and down variation eigenvectors are given by f^+, f^-. The decrease in the uncertainties of the shifted PDFs indicates the enhancement that including the FPF data in the global PDF fit could bring. Here, the profiling studies are performed using version 2.2.1 of the xFitter open-source QCD analysis framework [6–9], extended to support the use of PineAPPL grids [10,11]. Using the PDF4LHC21 [12] PDF set, the results are illustrated by comparing the fractional uncertainties of the original PDF set to those obtained after profiling. This is shown for the valence quark, gluon and the singlet distributions in Fig. 4.1 for FASERν2 pseudodata, while Fig. 4.2 indicates the impact of FASERν. FASERν2 is observed to provide tighter constraints on the PDFs, with the effects being the most prominent for the valence and sea quark distributions.

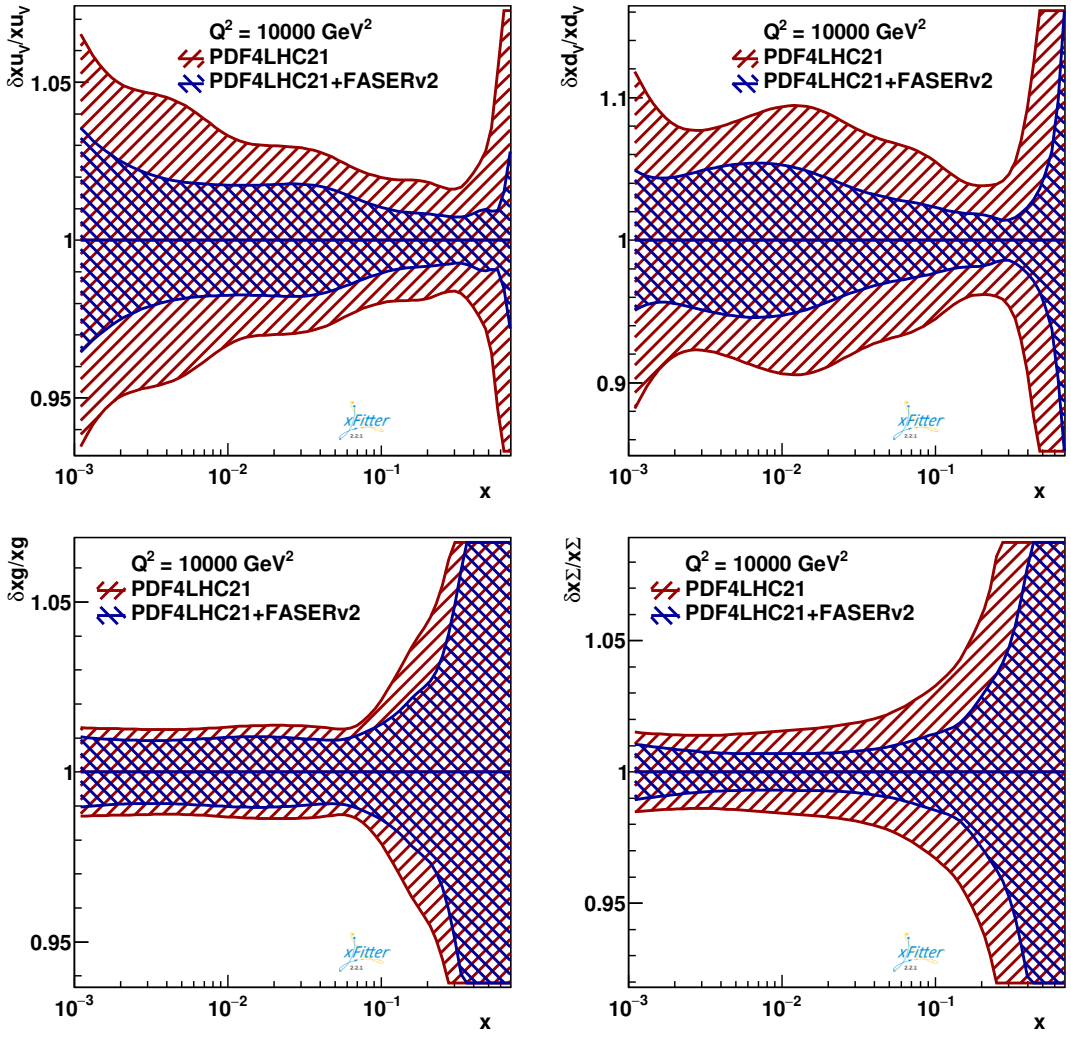

Figure 4.1. The fractional uncertainties in the valence quark, gluon and singlet PDFs as a function of the momentum fraction x at the scale $Q^2 = 10000\,\text{GeV}^2$. The profiling is performed using the PDF4LHC21 set and the pseudodata for FASERν2. The original uncertainty of PDF4LHC21 is indicated by the red band, while the blue band demonstrates the profiled result.

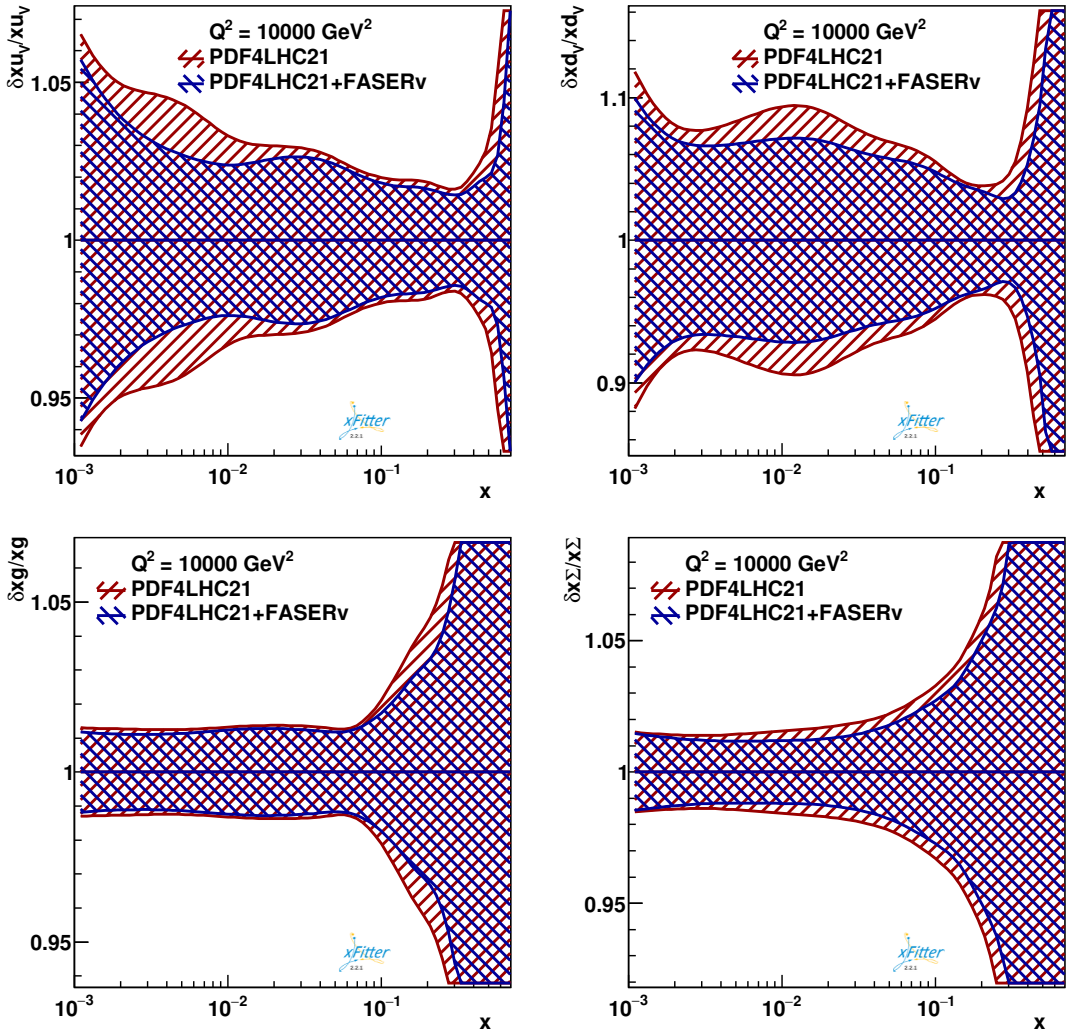

Figure 4.2. The fractional uncertainties in the valence quark, gluon and singlet PDFs as a function of the momentum fraction x at the scale $Q^2 = 10000\,\text{GeV}^2$. The profiling is performed using the PDF4LHC21 set and the pseudodata for FASERν. The original uncertainty of PDF4LHC21 is indicated by the red band, while the blue band demonstrates the profiled result.

5 Impact in nuclear PDF fits

Next we account for the nuclear dependence of the measured neutrino structure functions.

6 Description of the νFPF codes

The part that computes the differential cross sections is taken care by the python package νFPF. By default, it computes the HERA cross section defined as

$$\frac{d^2\tilde{\sigma}^A}{dxdy}\left(x,Q^2,y\right) = \frac{1}{2}\left[(1-y)F_2^{\nu A}(x,Q^2) + y^2 x F_1^{\nu A}(x,Q^2) + (-1)^\ell y\left(1-\frac{y}{2}\right)xF_3^{\nu A}(x,Q^2)\right], \tag{6.1}$$

where $\ell = 0$ for leptons and $\ell = 1$ for anti-leptons. Thus, in order to compare with Eq. 1.1 one needs to multiply the above equation with $G_F^2 s/2\pi(1+Q^2/m_W^2)^2$.

References

[1] F. Kling and L. J. Nevay, "Forward neutrino fluxes at the LHC," Phys. Rev. D **104** no. 11, (2021) 113008, arXiv:2105.08270 [hep-ph].

[2] H. Paukkunen and P. Zurita, "PDF reweighting in the Hessian matrix approach," JHEP **12** (2014) 100, arXiv:1402.6623 [hep-ph].

[3] C. Schmidt, J. Pumplin, C. P. Yuan, and P. Yuan, "Updating and optimizing error parton distribution function sets in the Hessian approach," Phys. Rev. D **98** no. 9, (2018) 094005, arXiv:1806.07950 [hep-ph].

[4] R. Abdul Khalek, S. Bailey, J. Gao, L. Harland-Lang, and J. Rojo, "Towards ultimate parton distributions at the high-luminosity LHC," Eur. Phys. J. C **78** (2018) 962, arXiv:1810.03639 [hep-ph].

[5] **HERAFitter developers' team** Collaboration, S. Camarda et al., "QCD analysis of W- and Z-boson production at Tevatron," Eur. Phys. J. C **75** no. 9, (2015) 458, arXiv:1503.05221 [hep-ph].

[6] S. Alekhin et al., "HERAFitter, open source QCD fit project," Eur. Phys. J. C **75** (2015) 304, arXiv:1410.4412 [hep-ph].

[7] V. Bertone, M. Botje, D. Britzger, et al., "xFitter 2.0.0: An open source QCD fit framework," PoS **DIS2017** (2018) 203, arXiv:1709.01151 [hep-ph].

[8] **xFitter** Collaboration, H. Abdolmaleki et al., "xFitter: An Open Source QCD Analysis Framework. A resource and reference document for the Snowmass study," 6, 2022. arXiv:2206.12465 [hep-ph].

[9] xFitter Developers' Team. https://www.xfitter.org/xFitter/.

[10] C. Schwan, A. Candido, F. Hekhorn, and S. Carrazza, "Nnpdf/pineappl: v0.5.9," Jan., 2023. https://doi.org/10.5281/zenodo.7499507.

[11] S. Carrazza, E. R. Nocera, C. Schwan, and M. Zaro, "PineAPPL: combining EW and QCD corrections for fast evaluation of LHC processes," JHEP **12** (2020) 108, arXiv:2008.12789 [hep-ph].

[12] **PDF4LHC Working Group** Collaboration, R. D. Ball et al., "The PDF4LHC21 combination of global PDF fits for the LHC Run III," J. Phys. G **49** no. 8, (2022) 080501, arXiv:2203.05506 [hep-ph].